Influence of ambient NO and NO₂ on the quantification of total peroxy nitrates ($\sum$PNs) and total alkyl nitrates ($\sum$ANs) by thermal dissociation cavity ring-down spectroscopy (TD-CRDS)

5 Laura Wüst[1], Patrick Dewald[1], Gunther N. T. E. Türk[1], Jos Lelieveld[1] and John N. Crowley[1]

[1]Atmospheric Chemistry Department, Max Planck Institute for Chemistry, Mainz, 55128, Germany

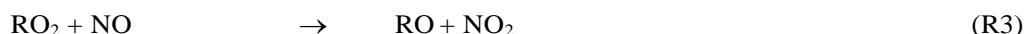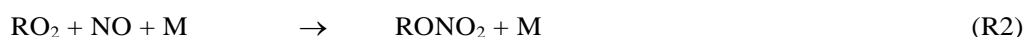*Correspondence to*: John N. Crowley (john.crowley@mpic.de)

Abstract

Measurement of total peroxy nitrates (ΣPNs) and alkyl nitrates (ΣANs) by instruments that use thermal dissociation (TD) inlets
10   to convert the organic nitrate to detectable NO_2 may suffer from systematic bias (both positive and negative) resulting from unwanted secondary chemistry in the heated inlets. Here we review the sources of the bias and the methods used to reduce it and/or correct for it and report new experiments using (for the first time) atmospherically relevant, unsaturated, biogenic alkyl nitrates as well as two different peroxyacetyl nitrate (PAN) sources. We show that the commonly used commercial C3-alkyl-nitrate (isopropyl nitrate, IPN) inlet for characterising the chemistry of ANs is not appropriate for real-air samples that contain
15   longer chain nitrates. ANs generated in the NO_3-induced oxidation of limonene are strongly positively biased in the presence of NO. By detecting NO_X rather than NO_2, we provide a simple solution to avoid the bias caused by the conversion of NO to NO_2 by primary and secondary peroxy radicals resulting from the complex chemistry in the thermal degradation of long-chain, alkyl nitrates in air at TD-temperatures. We also show that using a photochemical source of PAN to characterise the TD-inlets can result in a much stronger apparent bias from NO to NO_2 conversion than for a diffusion source of synthesised ("pure")
20   PAN at similar mixing ratios. This is explained by the presence of thermally labile trace gases such as peracetic acid ($CH_3C(O)OOH$) and hydrogen peroxide (H_2O_2).
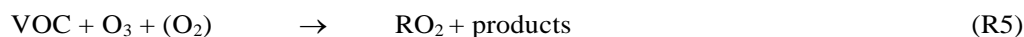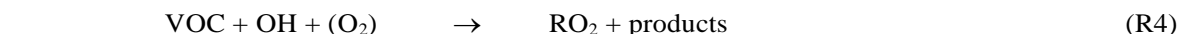
1 Introduction

Nitrogen monoxide (NO) and nitrogen dioxide (NO_2), together known as NO_X, have a significant impact on air quality and human health (Crutzen, 1979; Lelieveld et al., 2015). Measurements of trace gases that act as NO_x reservoirs or sinks are
25   essential to gain a deeper insight into the degradation and transport mechanisms of NO_X. Organic compounds with nitrate functionality, such as alkyl (aliphatic) nitrates (ANs, $RONO_2$) and peroxy nitrates (PNs, RO_2NO_2), influence the lifetime and transport of NO_X in the atmosphere (Horowitz et al., 2007; Perring et al., 2013) and represent a large fraction of the tropospheric nitrogen reservoir (Roberts, 1990). PNs are formed by the reaction between organic peroxy radicals (RO_2) and NO_2 (R1), while ANs are formed by the reaction between RO_2 and NO (R2) in competition with the formation of alkoxy radicals (R3), which
30   is usually the dominant reaction pathway (Orlando and Tyndall, 2012). PNs with a carbonyl group on the α-carbon, such as
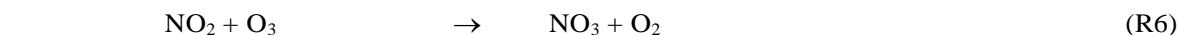
PAN, have lifetimes with respect to thermal dissociation to NO_2 of minutes to hours in the boundary layer, extending to years in the cold upper troposphere (Atkinson et al., 2006). In contrast, RO_2NO_2, which do not possess a α-carbonyl group decompose within seconds in the temperate boundary layer and these PNs have been detected only at ground level in polar regions (Slusher et al., 2002) or at high altitudes (Murphy et al., 2004).

35
$$RO_2 + NO_2 + M \quad \rightarrow \quad RO_2NO_2 + M \quad\quad\quad\quad (R1)$$
$$RO_2 + NO + M \quad \rightarrow \quad RONO_2 + M \quad\quad\quad\quad (R2)$$
$$RO_2 + NO \quad \rightarrow \quad RO + NO_2 \quad\quad\quad\quad (R3)$$

Organic peroxy radicals are formed during the day by the OH-initiated oxidation of volatile organic compounds (VOCs) (R4) (Lightfoot et al., 1992). During night, OH levels are much lower and the O_3-initiated oxidation of VOCs (R5) gains importance
40 as a source of RO_2 (Ng et al., 2017).

$$VOC + OH + (O_2) \quad \rightarrow \quad RO_2 + products \quad\quad\quad\quad (R4)$$
$$VOC + O_3 + (O_2) \quad \rightarrow \quad RO_2 + products \quad\quad\quad\quad (R5)$$
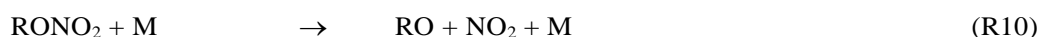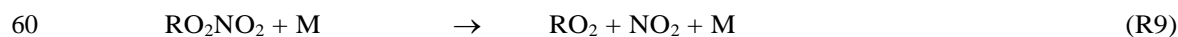
Nitrate radicals (NO_3) and dinitrogen pentoxide (N_2O_5) play important roles in atmospheric nitrogen chemistry, especially at nighttime (Brown and Stutz, 2012). The reaction of NO_2 with O_3 produces the NO_3 radical (R6), which is in thermal
45 equilibrium with NO_2 and N_2O_5 (R7) (Wayne et al., 1991).

$$NO_2 + O_3 \quad \rightarrow \quad NO_3 + O_2 \quad\quad\quad\quad (R6)$$
$$NO_2 + NO_3 + M \quad \rightleftharpoons \quad N_2O_5 + M \quad\quad\quad\quad (R7)$$

During the day, NO_3 is rapidly photolysed (Liebmann et al., 2018) or reacts with NO to form NO_2 (Wayne et al., 1991). At night, however, NO_3 can reach concentrations of up to several tens of pptv (Heintz et al., 1996; Geyer et al., 2001; Brown et
50 al., 2003; Dewald et al., 2022) and initiates the oxidation of many unsaturated VOCs (R8), especially terpenoids (Ng et al., 2017). In environments with high levels of biogenic VOCs, NO_3 also contributes to their oxidation during the day (Liebmann et al., 2019; Dewald et al., 2024).

$$NO_3 + VOC + (O_2) \quad \rightarrow \quad RONO_2 + products \quad\quad\quad\quad (R8)$$
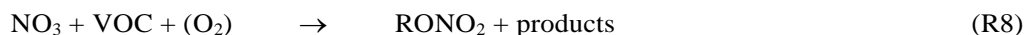
PNs and ANs have often been measured using chromatographic (Flocke et al., 2005) and mass spectrometric methods
55 (Slusher et al., 2004; Zheng et al., 2011; Wu et al., 2021) that allow identification and quantification of the individual components. An alternative method for measuring total, non-speciated PNs and ANs (i.e. $\sum$PNs and $\sum$ANs) is thermal dissociation to NO_2 (R9-R10) and subsequent detection by cavity ring-down spectroscopy (TD-CRDS) or laser induced fluorescence (TD-LIF) (Day et al., 2002; Paul et al., 2009; Paul and Osthoff, 2010; Sobanski et al., 2016; Thieser et al., 2016).

60
$$RO_2NO_2 + M \quad \rightarrow \quad RO_2 + NO_2 + M \quad\quad\quad\quad (R9)$$
$$RONO_2 + M \quad \rightarrow \quad RO + NO_2 + M \quad\quad\quad\quad (R10)$$

This method makes use of the very different bond-strengths of $ROO-NO_2$ and $RO-NO_2$ to separate their detection in inlets at appropriate temperatures (Day et al., 2002), typically around 473 K for PNs and 673 K for ANs for instruments developed in
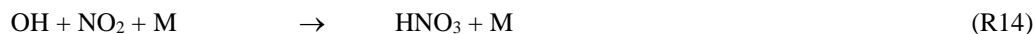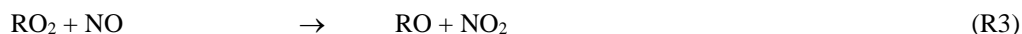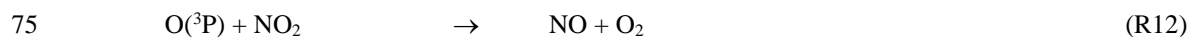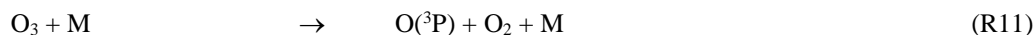
this group for example (Sobanski et al., 2016; Thieser et al., 2016). As discussed below, the thermal dissociation of PNs and

65   ANs to NO_2 can however result in deviation from ideal (1:1) conversion as a result of unwanted, secondary chemistry.

2 Sources of potential bias in TD-CRDS measurements of PNs and ANs

The quantitative measurement of $\sum$ANs and $\sum$PNs as NO_2 following thermal dissociation can be influenced by secondary reactions that either generate or consume the NO_2 product. The origin of the bias and the various methods that have been used to reduce it or correct for it are summarised below.

70   The three types of reactions that can modify the concentration of NO_2 formed in thermal dissociation of $\sum$ANs or $\sum$PNs are its reduction to NO (R11-R12), the oxidation of ambient NO to NO_2 via reaction with O_3 or with RO_2 formed in the TD-inlet (R3, R13) and the conversion of NO_2 back to an organic/inorganic nitrate (R14, R15) (Day et al., 2002; Paul et al., 2009; Paul and Osthoff, 2010; Di Carlo et al., 2013; Sobanski et al., 2016; Thieser et al., 2016).

$O_3 + M$	$\rightarrow$	$O(^3P) + O_2 + M$	(R11)
$O(^3P) + NO_2$	$\rightarrow$	$NO + O_2$	(R12)
$O_3 + NO$	$\rightarrow$	$O_2 + NO_2$	(R13)
$RO_2 + NO$	$\rightarrow$	$RO + NO_2$	(R3)
$OH + NO_2 + M$	$\rightarrow$	$HNO_3 + M$	(R14)
$RO_2 + NO_2 + M$	$\rightarrow$	$RO_2NO_2 + M$	(R15)

80   The size of the bias caused by these reactions depends sensitively on characteristics of the heated inlet, in particular the pressure at which it is operated. Instruments that use CRDS setups to detect NO_2 are usually operated at cavity pressures (and thus inlet pressures) above 500 hPa, whereas the TD-inlets of instruments using LIF to detect NO_2 can be operated at any pressure above that of the LIF-module, which is typically at 3-5 hPa (Day et al., 2002). Operation at low pressures is generally preferred as it enhances the rate of diffusive loss of radicals to the inlet walls, minimising the bias. A potential disadvantage of operation at

85   low temperatures is the enhancement of the $O(^3P)$ concentration as its (termolecular) reaction with O_2 (the reverse of R11) to reform O_3 is greatly reduced (Lee et al., 2014). Recognising that many of the secondary processes involve radicals and atoms formed in the heated inlets, Sobanski et al. (2016) added glass beads in the TD-section of the inlet of their CRD-based device to scavenge peroxy and OH radicals. While this successfully reduced the impact of $O(^3P)$, OH and RO_2 radical reactions (reducing the observed bias), the use of glass beads with a large surface area was later shown to reduce the temperature at

90   which unsaturated (e.g. biogenic) ANs are converted to NO_2 in the presence of O_3, resulting in the partial detection of ANs in the PNs channel with an inlet at 473 K (Dewald et al., 2021). This effect was weaker, but still apparent when using a quartz inlet without glass beads. This observation led Dewald et al. (2021) to switch to a Teflon (PFA) inlet which does not support the formation of reactive surface sites (S-O) that calalyse the multistep conversion of ANs to NO_2. Note that such effects are not observed for saturated ANs (e.g. isopropyl nitrate, which has often been used as easily available "standard" to test inlet

95   effects), which do not react with O_3.

An alternative approach to the physical reduction of bias (e.g. by removing radicals in the TD-inlet) is a correction based on laboratory characterisation of the effects of adding O_3, NO and NO_2 to the inlets in the presence of PNs and ANs followed by numerical simulation of the results using reaction schemes that describe the gas-phase and heterogeneous reactions taking place (Sobanski et al., 2016; Thieser et al., 2016).

100 Table 1 presents a summary of the bias measured by various groups using TD-inlets coupled to various NO_2 detection schemes and the approaches used to minimise and /or correct them.

Table 1: Overview of the bias from secondary chemistry occuring when using TD-inlets and various detection methods for NO_2.

Process	TD-Inlet	Method	Organic Nitrate	Bias	Size of bias	Corrective approach	Reference
$O(^3P) + NO_2$	>603 K	LIF	--	-ve	< 3.5 % loss of NO_2 (200 – 240 ppbv O_3)	--	Day et al. (2002)
$O(^3P) + NO_2$	653 K	LIF	--	-ve	6 % loss of NO_2 (30 ppbv O_3)	a) Expression based on laboratory data	Lee et al. (2014)
$O(^3P) + NO_2$	723 K	CRDS	--	-ve	< 4 % loss of NO_2 (50 ppbv O_3)	b) Expression based on laboratory data	Thieser et al. (2016)
$O(^3P) + NO_2$	648 K	CRDS	--	-ve	1.5 % loss of NO_2 (50 ppbv O_3)	Glass beads, numerical simulation	Sobanski et al. (2016)
$O(^3P) + NO_2$	653 K	CEAS	--	-ve	Not significant	--	Li et al. (2021)
$O_3 + NO$	873 K	LIF	--	+ve	1.6 % of the NO converted to NO_2 (100 ppbv O_3)	Bias quantified in laboratory data	Day et al. (2002)
$O_3 + NO$	673 K	LIF	--	+ve	< 1 % of the NO	Reduced pressure (< 5 HPa), numerical simulation.	Wooldridge et al. (2010)
$O_3 + NO$	473 K 723 K	CRDS	--	+ve	0.13 ppbv (1 ppbv NO and 50 ppbv O_3) 0.33 ppbv (1 ppbv NO and 50 ppbv O_3)	c) Expression based on laboratory data	Thieser et al. (2016)
$O_3 + NO$	448 K 648 K	CRDS	--	+ve	1.0 ppbv (1 ppbv NO and 50 ppbv O_3) 1.7 ppbv (1 ppbv NO and 50 ppbv O_3)	Glass beads, numerical simulation	Sobanski et al. (2016)
$O_3 + NO$	453 K 653 K	CEAS	--	+ve	Not significant (within the measurement uncertainty)	--	Li et al. (2021)
$RO_2 + NO$	523 K	CRDS	PAN	+ve	Factor 1.20 (1 ppbv PAN and 4 ppbv NO)	Second order polynomial expression based on laboratory data	Paul and Osthoff (2010)
$RO_2 + NO$	473 K	LIF	PAN	+ve	< Factor 1.05 (NO < 3 ppbv)	Reduced pressure (< 5 HPa), numerical simulation.	Wooldridge et al. (2010)
$RO_2 + NO$	463 K	CIMS	PPN	-ve	Factor 2 (2.2 ppbv PPN and 5 ppbv NO)	Laboratory data. Suppression of ion signal from matrix effects.	Mielke and Osthoff (2012)
$RO_2 + NO$	473 K	CRDS	PAN	+ve	Factor 1.80 (1 ppbv PAN and 4 ppbv NO)	Numerical simulation	Thieser et al. (2016)
$RO_2 + NO$	723 K	CRDS	PAN	+ve	Factor 1.25 (1 ppbv PAN and 4 ppbv NO)	Numerical simulation	Thieser et al. (2016)
$RO_2 + NO$	448 K	CRDS	PAN	+ve	Factor 1.40 (3 ppbv PAN and 8 ppbv NO)	Glass beads, numerical simulation	Sobanski et al. (2016)
$RO_2 + NO$	648 K	CRDS	PAN	+ve	Factor 1.04 (3 ppbv PAN and 8 ppbv NO)	Glass beads, numerical simulation	Sobanski et al. (2016)
$RO_2 + NO$	433 K 633 K	CAPS	--	+ve	Not mentioned	--	Sadanaga et al. (2016)
$RO_2 + NO$	523 K	PERCA-CRDS	PAN	+ve	Factor 4.0 (2 ppbv PAN and 0.75 ppmv NO)	Numerical simulation	Taha et al. (2018)
$RO_2 + NO$	403 K	CAPS	--	+ve	Not determined	Numerical simulation	Keehan et al. (2020)
$RO_2 + NO$	453 K	CEAS	PAN	+ve	Factor 1.56 (2.8 ppbv PAN and 5 ppbv NO)	Numerical simulation	Li et al. (2021)
$RO_2 + NO$	653 K	CEAS	PAN	+ve	Factor 1.40 (2.8 ppbv PAN and 5 ppbv NO)	Numerical simulation	Li et al. (2021)
$RO_2 + NO$	453 K	CRDS	PAN	+ve	Factor 1.12 (2.11 ppbv PAN and 5 ppbv NO)	Glass beads	Lin et al. (2024)
$RO_2 + NO$	633 K	CRDS	PAN	+ve	Not significant	Glass beads, laboratory data	Lin et al. (2024)
$RO_2 + NO$	433 K	CAPS	PAN	+ve	Factor 4.10 (0.8 ppbv PAN and 8.5 ppbv NO)	Detection of NO_X	Ohara et al. (2024)
$RO_2 + NO$	448 K	CRDS	PAN	+ve	Factor 1.55 (2 ppbv PAN and 4 ppbv NO).	Detection of NO_X	This work
$RO_2 + NO$	648 K	CRDS	PAN	+ve	Factor 1.70 (2 ppbv PAN and 4 ppbv NO).	Detection of NO_X	This work
$RO_2 + NO$	673 K	LIF	NPN	+ve	0.7 % conversion of NO to NO_2 per ppbv of AN	Reduced pressure (2.7-5.3 HPa)	Day et al. (2002)
$RO_2 + NO$	723 K	CRDS	IPN	+ve	1.6 % conversion of NO to NO_2 per ppbv of AN	Numerical simulation	Thieser et al. (2016)
$RO_2 + NO$	648 K	CRDS	IPN	+ve	Factor 1.2 (1.4 ppbv IPN and 6 ppbv NO)	Glass beads, numerical simulation	Sobanski et al. (2016)
$RO_2 + NO$	653 K	CEAS	MN	+ve	Not mentioned	Numerical simulation	Li et al. (2021)
$RO_2 + NO$	633 K	CRDS	EHN	+ve	Factor 1.12 (3.36 ppbv EHN and 6 ppbv NO)	Glass beads, standard addition experiments	Lin et al. (2024)
$RO_2 + NO$	633 K	CAPS	IPN	+ve	Factor 2.8 (0.97 ppbv IPN and 6 ppbv NO)	Detection of NO_X	Ohara et al. (2024)

RO_2 + NO	648 K	CRDS	Limonene-nitrate	+ve	25 % conversion of NO to NO_2 per ppbv of AN	Detection of NO_X	This work
RO_2 + NO	648 K	CRDS	Isoprene-nitrate	+ve	5.1 % conversion of NO to NO_2 per ppbv of AN	Detection of NO_X	This work
RO_2 + NO_2	523 K	CRDS	PAN	-ve	Not significant	--	Paul et al. (2009)
RO_2 + NO_2	473 K	LIF	PAN	-ve	> Factor 1.05 (NO_X < 3 ppbv)	Simulations and operate at a pressure of < 5 Hpa	Wooldridge et al. (2010)
RO_2 + NO_2	463 K	CIMS	PPN	-ve	Factor 1.25 (2.2 ppbv PPN and 5 ppbv NO)	Laboratory data. Suppression of ion signal from matrix effects	Mielke and Osthoff (2012)
RO_2 + NO_2	473 K	LIF	PAN	-ve	3 pptv per ppbv NO_2		Di Carlo et al. (2013)
RO_2 + NO_2	473 K	CRDS	PAN	-ve	Factor 1.52 (0.7 ppbv PAN and 8 ppbv NO_2)	Numerical simulation	Thieser et al. (2016)
RO_2 + NO_2	723 K	CRDS	PAN	-ve	Not significant	--	Thieser et al. (2016)
RO_2 + NO_2	448 K	CRDS	PAN	-ve	Factor 1.06 (9 ppbv PAN and 8 ppbv NO_2)	Numerical simulation	Sobanski et al. (2016)
RO_2 + NO_2	648 K	CRDS	PAN	-ve	Not significant	--	Sobanski et al. (2016)
RO_2 + NO_2	403 K	CRDS	Carene-nitrate	-ve	Factor 2.33 (1 ppbv PNs and 10 ppbv NO_2)	Numerical simulation	Keehan et al. (2020)
RO_2 + NO_2	453 K	CEAS	PAN	-ve	Factor 1.43 (3.3 ppbv PAN and 10.5 ppbv NO_2)	Numerical simulation	Li et al. (2021)
RO_2 + NO_2	653 K	CEAS	PAN	-ve	Factor 1.08 (3.3 ppbv PAN and 10.5 ppbv NO_2)	Numerical simulation	Li et al. (2021)
RO_2 + NO_2	453 K	CRDS	PAN	-ve	Factor 1.15 (2.8 ppbv PAN and 10 ppbv NO_2)	Glass beads, standard addition experiments	Lin et al. (2024)
RO_2 + NO_2	633 K	CRDS	PAN	-ve	Factor 1.04 (1.71 ppbv PAN and 10 ppbv NO_2)	Glass beads, standard addition experiments	Lin et al. (2024)
RO_2 + NO_2	448 K	CRDS	PAN	-ve	Factor 1.61 (2 ppbv PAN and 11 ppbv NO_2)	Numerical simulation	This work
RO_2 + NO_2	648 K	CRDS	PAN	-ve	Factor 1.08 (2 ppbv PAN and 11 ppbv NO_2)	Numerical simulation	This work
RO_2 + NO_2	723	LIF	EN	-ve	Not significant	--	Di Carlo et al. (2013)
RO_2 + NO_2	723 K	CRDS	IPN	-ve	Factor 1.05 (12 ppbv NO_2)	Numerical simulation	Thieser et al. (2016)
RO_2 + NO_2	648 K	CRDS	IPN	-ve	Factor 1.03 (6 ppbv NO_2)	Numerical simulation	Sobanski et al. (2016)
RO_2 + NO_2	633 K	CRDS	EHN	-ve	Factor 1.27 (2.03 ppbv EHN and 12 ppbv NO_2)	Glass beads, standard addition experiments	Lin et al. (2024)
RO_2 + NO_2	648 K	CRDS	Limonene-nitrate	-ve	Upper limit: Factor 1.09 (3.37 ppbv Limonene-nitrate and 20 ppbv NO_2)	--	This work
RO_2 + NO_2	433 K 633 K	CAPS	PAN IPN	-ve	Not significant	--	Ohara et al. (2024)

Notes:

CRDS = cavity ring-down-spectroscopy, CAPS = cavity attenuated phase shift spectroscopy, CEAS = cavity-enhanced absorption spectroscopy, CIMS = chemical ionization mass spectrometry, LIF = laser induced fluorescence, PERCA = peroxy radical amplifier. PAN is $CH_3C(O)OONO_2$, PPN is $C_2H_5C(O)OONO_2$, IPN is isopropyl nitrate (($CH_3)_2CH_2ONO_2,CH_3$), MN is methyl-nitrate (CH_3ONO_2), EN is ethyl-nitrate ($C_2H_5ONO_2$), NPN is n-propyl-nitrate ($CH_3CH_2CH_2ONO_2$), EHN is 2-ethylhexyl-nitrate. a) $S'_{380} = S_{380} / (0.0694 \times \ln(S_{380}) - 0.308) \times (0.0115 \times [O_3] + 0.557)$ where S_{380} is the observed total signal and S'_{380} is the corrected signal. b) NO_2 loss (L_{NO2} (ppbv) = 7.43×10^{-4} [NO_2][O_3]). c) k_{eff}(473 K) = 2.5×10^{-14} cm^3 molecule^{-1} s^{-1}, k_{eff}(723 K) = 6.2×10^{-14} cm^3 molecule^{-1} s^{-1} where k_{eff} is an effective rate coefficient for the reaction between O_3 and NO.

In this study we assess the bias caused by ambient NO on $\sum$PNs and $\sum$ANs measurements, with a focus on biogenically derived ANs formed in the NO_3-induced oxidation of isoprene and limonene, which so far have been neglected in the studies reviewed in Tab. 1. We show that the use of unsaturated surrogate alkyl-nitrates (e.g. IPN) to estimate bias in TD-inlets leads to a different effect compared to alkyl nitrates derived from the oxidation of common biogenic trace gases such as terpenoids and as such is inappropriate for estimating and correcting bias.

3 Experimental

3.1 TD-Cavity ring-down spectrometer

The measurements were performed using a 5-channel cavity ring-down spectrometer, which has been described in detail
120 previously (Sobanski et al., 2016; Dewald et al., 2021). In this study, we use only the three cavities that detect NO_2. Each cavity consists of a stainless steel tube (70 cm length and inner diameter 8 mm) that is internaly coated with Teflon (Chemours, FEP, TE 9568) to reduce losses of trace-gases during transmission. Perfluoroalkoxy polymer (PFA) T-pieces at both ends of the tubes provide connections to the sample inlet-line (see Fig. 1) and the outlet to the pump. Sample air enters the cavities at a flow rate of 2.1 slpm in each channel. Two highly reflective mirrors (transmission of 20 ppm at 409 nm, FiveNine Optics)
125 are located behind each PFA T-piece at a distance of 93.5 cm (d) apart. The mirrors are purged with dry zero air (CAP 180, Fuhr GmbH) which results in a reduction of the effective optical path length, l, compared to the mirror distance. To record a ring-down signal, light emitted by a laser diode is coupled into the cavities using 50 µm core optical fibres and collimators. Using a photomultiplier tube, which converts the transmitted light intensity into an analogue electrical signal, an exponential decay can be observed when the laser is temporarily switched off. The concentration of NO_2 in each cavity is calculated from:

$$130 \quad [NO_2] = \frac{d}{l} \frac{(k-k_0)}{c \cdot \sigma_\lambda}, \tag{1}$$

where k_0 and k are the decay rate coefficients without and with absorbing/scattering medium, c is the speed of light and σ_λ is the effective absorption cross section resulting from the overlap of the laser emission and the NO_2 absorption spectrum (Vandaele et al., 1998).
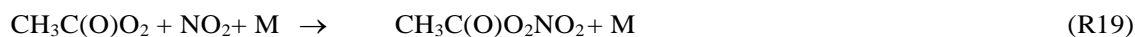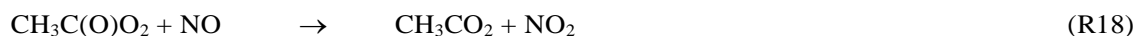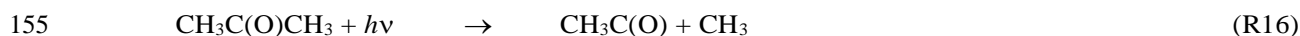
In the original version of this instrument (Sobanski et al., 2016; Dewald et al., 2021), three cavities were operated at 409 nm
135 to detect either NO_2 or $\sum PNs + NO_2$ or $\sum ANs + \sum PNs + NO_2$. We refer to these as the "NO_2-cavity", the "PNs-cavity" and the "ANs-cavity", respectively. The NO_2-cavity sampled air via a 60 cm long PFA inlet (8 mm inner diameter) at ambient temperature. The PNs-cavity sampled via a 55 cm long PFA tubular (8 mm inner diameter), the first 20 cm of which were heated to 448 K to convert PNs to NO_2. The ANs-cavity sampled air via a 55 cm long quartz tube (12 mm inner diameter), where the first 20 cm were heated to 648 K, to convert ANs to NO_2.

140 In this work, we examine the advantages of detecting NO_X rather than NO_2 when using a TD-CRDS to measure peroxy nitrates and alkyl nitrates derived from biogenic precursors. The instrument was modified to detect NO_X by adding O_3 (Fig. 1) which was generated by passing zero air over a low-pressure Hg-lamp emitting at 185 nm. The O_3 was divided equally by critical orifices into three identical reaction volumes made of 88 cm long PFA tubing (0.5 inch outer diameter, residence time of 1.8 s). About 12 ppmv O_3 were needed to fully convert NO to NO_2. This was determined experimentally by changing the flow
145 through the critical orifices while monitoring NO_2 for a fixed amount of NO. A numerical simulation of the reactions describing the formation and loss of NO_2 (Fig. S1) indicated a conversion efficiency of 98.7 %.

3.2 PAN sources

Two different sources of PAN were used in this study. In the first, PAN was prepared via the photolysis of acetone in air in the presence of NO as described originally by Warneck and Zerbach (1992) and improved by e.g. Flocke et al. (2005). In this

150 case, 5 sccm of acetone (4.6 % in synthetic air, Air Liquide) and 10 sccm of NO (1 ppmv, Air Liquide) were mixed with 100 sccm of zero air before flowing into a quartz reactor equipped with a phosphor-coated, low-pressure mercury lamp (Pen-Ray) to photolyse acetone at ~ 285 nm (R16). Based on the volume flow rate and the volume of the reactor (~ 243 cm^3), the residence time of the gas flowing through the reactor was calculated to be ~ 120 s. PAN is formed at a yield of ~ 90-95 % (relative to NO consumed) by the sequence of reactions (R16-R19).

155 $\qquad$ $CH_3C(O)CH_3 + h\nu$ $\qquad \rightarrow \qquad$ $CH_3C(O) + CH_3$ $\hfill$ (R16)

$\qquad$ $CH_3C(O) + O_2 + M$ $\qquad \rightarrow \qquad$ $CH_3C(O)O_2 + M$ $\hfill$ (R17)

$\qquad$ $CH_3C(O)O_2 + NO$ $\qquad \rightarrow \qquad$ $CH_3CO_2 + NO_2$ $\hfill$ (R18)

160

$\qquad$ $CH_3C(O)O_2 + NO_2 + M \rightarrow$ $\quad$ $CH_3C(O)O_2NO_2 + M$ $\hfill$ (R19)

The mixture exiting the photochemical reactor was diluted with 5.2 slpm zero air to provide PAN mixing ratios of 1.7 ppbv. In order to ensure a known concentration of PAN, such photochemical PAN-sources are operated in the NO-limited chemical

165 regime, i.e. sufficent peroxyl radicals are present to initially convert a NO to NO_2 and then to PAN. High radical densities implies that other chemical processes involving peroxyl radicals take place. In section 4.1, we later discuss the concentrations and role of the organic and inorganic photochemical products other than PAN that are generated in the reactor.

Alternatively, PAN was synthesised using wet-chemical methods (Gaffney et al., 1984; Talukdar et al., 1995). Tridecane (10 mL, ≥ 99 %, Sigma-Aldrich) and peroxyacetic acid (PAA) (2.5 mL, 35 % by weight in dilute acetic acid, Acros Organics)

170 were placed in a 100 mL wide-necked round-bottom flask and cooled to 273 K in an ice-water bath. Cold sulphuric acid (2.5 mL, 98 %, Roth) and then cold nitric acid (1.3 mL, ≥ 65 %, Sigma-Aldrich) were added dropwise while stirring. The contents of the flask were allowed to stand for 25 minutes at 273 K with vigorous stirring and then transferred to a separatory funnel containing ice-cold Milli-Q water (25 mL). The aqueous phase was discarded and the organic phase was shaken four times with 25 mL of cold Milli-Q water each time. The organic phase was then dried for 30 minutes at 273 K with magnesium

175 sulphate (1 spatula, Alfa Aesar). After filtration, PAN was obtained as a colourless liquid in tridecan and stored at 243 K until use. During experiments, PAN was cooled to 273 K in a cryostat and eluted into the gas-phase by flowing 100 sccm of air over the sample, with further dilution with 5.2 slpm zero air resulting in mixing ratios between 2.0 and 6.5 ppbv.

3.3 AN sources

Limonene nitrates and isoprene nitrates were formed by the reaction of limonene or isoprene with NO_3 in air in the 1 m^3

180 simulation chamber SCHARK (Simulation Chamber for Atmospheric Reactions and Kinetics), which was operated at ambient

7

pressure and temperature (1 atm, 298 K) in dynamic-flow mode (Dewald et al., 2021). Residence times in the chamber were between 57 and 92 minutes depending on the flow rate. Gases entering the chamber passed through a circular loop of PFA tubing (located at the bottom of the chamber) with 10, equally spaced, 1 mm-diameter holes pointing upwards. The velocity of gas at the exit of the holes is estimated at ~2 m s^{-1}, which causes rapid turbulent mixing. Mixing is also assisted by a ~5 cm

185 diameter, teflon coated fan located centrally at the bottom of the chamber. Experiments with pulsed addition of O_3, showed that the mixing time in the chamber was < 40 s, which is negligible compared to the overal residence time.

Two methods were used to produce NO_3. In the first, NO_3 was formed by the thermal decomposition of N_2O_5 (R7) which was eluted into the chamber by passing zero air (50 - 600 sccm) over N_2O_5 crystals held at temperatures between 205 K and 195 K (acetone-dry ice bath). N_2O_5 was synthesised by flowing 150 sccm of NO (5% in N_2, Westfalen) and 200 sccm of O_3 in O_2 (~

190 10 % O_3, generated via electrical discharge in O_2) through a ~ 2 L, glass reaction vessel and trapped as colourless crystals at 195 K (acetone-dry ice bath). N_2O_5 crystals formed this way were stored at 243 K until use. Alternatively, NO_3 was obtained by bubbling 50-200 sccm of zero air through a 0.5 M solution of cerium(IV) ammonium nitrate (CAN in 6 M HNO_3) that was irradiated at 365 nm (Lambe et al., 2023). The flow containing the NO_3 was diluted by 15 slpm zero air before entering the chamber. The thermal decomposition of N_2O_5 has the advantage that the lifetime of N_2O_5 is sufficiently long (~23 s at 298 K)

195 to ensure that NO_3 is formed reasonably homogeneously throughout the chamber. The disadvantage of using N_2O_5 is the release of NO_2 during its thermal decomposition. The photochemical CAN source suffers from the disadvantage that the NO_3 (added via a point source) may react before mixing is complete. i.e. the lifetime of NO_3 in the presence of (typically) 30 ppbv of limonene or isoprene is only 0.1 -2 s, which is shorter than the mixing time. Isoprene and limonene were introduced into the chamber via flow-controllers attached to steel canisters containing isoprene (98%, Acros Organics, 45 ppmv in He) or limonene

200 (96%, Sigma-Aldrich, 44 ppmv in He) in He (5.0, Westfalen), resulting in ANs mixing ratios between 0.47 and 4.4 ppbv.

The nitrates generated in this manner from isoprene are a mixture of C5-nitrooxyhydroperoxides, C5-nitrooxycarbonyl, C5-hydroxynitrate and also C10-nitrooxyperoxide (ROOR), with the relative concentrations depending on the fate of the initially formed nitrooxyperoxy radicals (IUPAC 2024). The limonene nitrates formed are mainly C10-hydroxynitrates at yields of ~ 20 % (Spittler et al., 2006).

205 **3.4 Experimental procedure**

In order to investigate the influence of NO and NO_2 on the detection of PAN and biogenically derived ANs via TD-CRDS, different amounts of NO (0 – 22.5 ppbv) and NO_2 (0 – 20 ppbv) were added to the TD-inlet of the CRDS along with various amounts of PAN, isoprene-derived ANs and limonene-derived ANs. These experiments were carried out with the cavities operating both in "NO_2-mode" and in "NO_X-mode" by adding O_3 (see section 3.2).

4 Results and discussion

4.1 The influence of NO on the measurement of PNs (Photochemical PAN source, PAN measured as NO_2)

The presence of NO during the measurement of PNs using TD-inlets leads to a positive bias in ambient PNs concentration, which is related to the oxidation of NO to NO_2 via reactions with peroxyl radicals (see section 2) (Sobanski et al., 2016; Thieser et al., 2016). To re-investigate this measurement artefact, extend previous studies from this group and provide a solution to improve the reliability of TD-CRDS instruments designed to measure ΣPNs, we have performed experiments using both a photochemical source and a diffusion PAN source (see section 3.2). Fig. 2 summarises the results of an experiment in which NO was added to photochemically produced PAN (≈ 1.7 ppbv). In these experiments, O_3 was NOT added to the tubing in front of the cavities (low-pressure Hg-lamp off) so that the cavities detected NO_2 (and not NO_X). The mixing ratios of NO_2 measured in the cavities with inlet temperatures of 448 and 648 K are plotted against the amount of NO added, which was calculated from its partial flow and mixing ratio in the bottle (1 ppmv in N_2). For both datasets, the NO_2 measured in the room temperature cavity (present as an impurity in the PAN sample) has already been subtracted.

Ideally, only one molecule of NO_2 would be generated for each PAN molecule thermally dissociated and the data would describe a horizontal line at ~1.7 ppbv. As Fig. 2a shows this is clearly not the case. In both cavities with heated inlets the addition of NO leads to the formation of additional NO_2. This is related to co-formation of the acetyl peroxy radical from PAN in the heated inlet at 448 K (R20) which reacts with NO (R21) to form NO_2 and (in air) a methyl peroxy radical (R21a-b). The methyl peroxy radical can react with NO to form a further NO_2 and HO_2 (R22); the latter can form a third NO_2 in the reaction between HO_2 and NO (R23). The OH radical formed in this process reacts either with NO to form HONO or with NO_2 to form HNO_3 both of which resist dissociation in the 448 K TD-inlet (Thieser et al., 2016; Friedrich et al., 2020).

$$CH_3C(O)O_2NO_2 + M \rightarrow CH_3C(O)O_2 + NO_2 + M \qquad (R20)$$
$$CH_3C(O)O_2 + NO \rightarrow CH_3CO_2 + NO_2 \qquad (R21)$$
$$CH_3CO_2 + M \rightarrow CH_3 + CO_2 + M \qquad (R21a)$$
$$CH_3 + O_2 + M \rightarrow CH_3O_2 + M \qquad (R21b)$$
$$CH_3O_2 + NO + (O_2) \rightarrow HCHO + HO_2 + NO_2 \qquad (R22)$$
$$HO_2 + NO \rightarrow OH + NO_2 \qquad (R23)$$

Additionally, the radicals involved (e.g. RO_2, RO, OH) can be lost to the walls of the TD-inlet, which modifies the extent of the conversion of NO to NO_2. In our experiments with a TD-inlet at 448 K and 1.7 ppbv PAN, the addition of 20 ppbv NO results in detection of > 5 ppbv NO_2. At this temperature, the increase in NO_2 per NO added is lower at high NO than at low NO (i.e. the curve flattens at high NO).

At 648 K the chemistry is different as the acetyl-peroxy radical decomposes into an acetyl radical and oxygen (R24) or isomerises to $CH_2C(O)OOH$ (R25) (Lee et al., 2002; Carr et al., 2011; Thieser et al., 2016) which decomposes thermally to OH and a singlet α-lactone (R26) (Carr et al., 2011; Thieser et al., 2016). The acetyl radical from equation R24 can decompose to CH_3 and CO (R27), react with O_2 to form an acetyl peroxy radical (R28) or form OH and the singlet α-lactone (R29) (Tyndall

et al., 1995; Carr et al., 2007; Chen and Lee, 2010; Carr et al., 2011; Groß et al., 2014; Papadimitriou et al., 2015; Thieser et al., 2016). The methyl radical formed in equation (R27) reacts with oxygen to form a methyl peroxy radical (R21b), which
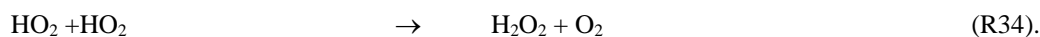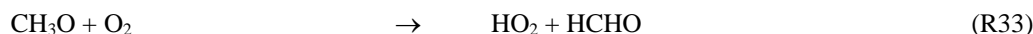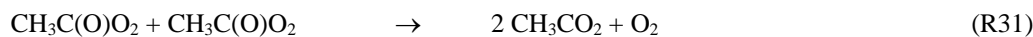
245 reacts with NO to form NO_2 (R22).

$$CH_3C(O)O_2 + M \quad \rightarrow \quad CH_3C(O) + O_2 + M \qquad \text{(R24)}$$

$$CH_3C(O)O_2 + M \quad \rightarrow \quad CH_2C(O)OOH + M \qquad \text{(R25)}$$

$$CH_2C(O)OOH \quad \rightarrow \quad {}^1C_2H_2O_2 + OH \qquad \text{(R26)}$$

$$CH_3C(O) \quad \rightarrow \quad CH_3 + CO \qquad \text{(R27)}$$

250
$$CH_3C(O) + O_2 + M \quad \rightarrow \quad CH_3C(O)O_2 + M \qquad \text{(R28)}$$

$$CH_3C(O) + O_2 \quad \rightarrow \quad {}^1C_2H_2O_2 + OH \qquad \text{(R29)}$$

For the 648 K inlet the bias is even larger (a factor >5 increase in NO_2 going from zero to 20 ppbv NO) and appears to flatten-off more slowly. This result was unexpected as previous studies from this laboratory have indicated that at high temperatures, the bias is weaker owing to thermal decomposition of $CH_3C(O)O_2$.

255 In order to explore this effect, a thermogram of the photochemical PAN source was measured while continuously adding 13 ppbv of NO to the TD-inlet. The result is displayed in Fig. 3, which confirms that NO to NO_2 conversion continues past the PAN-maximum close to 440 K with a doubling of the NO_2 mixing ratio at 648 K.

In order to understand the origin of the additional NO_2 signal at high temperatures, a further experiment was carried out in which the photochemical PAN source was switched on, but without adding NO to produce PAN. This can be seen in Fig. 2b

260 and shows that the conversion of NO to NO_2 in the 648 K cavity continues despite the absence of PAN and thus cannot be explained solely by reactions initiated by formation of the acetyl peroxy radical. A smaller conversion of NO to NO_2 is also observed in the 448 K cavity in the absence of PAN.

In the absence of NO, peroxy radicals formed by acetone photolysis in the photochemical reactor undergo a series of self- and cross-reactions that lead to a number of organic end-products that can be transported from the photochemical reactor to the

265 TD-inlets. Note that within the photochemical reactor significant concentrations of hydroxy- and peroxy-radicals are only present in the steady-state when irradiated and do not survive transport through the tubing ($\approx$ 2 m of ¼ inch PFA) to the TD-inlets.

The two initially formed peroxyl radicals (R16-17 and R21b) $CH_3C(O)O_2$ and CH_3O_2 can undergo self- and cross-reactions in the photochemical reactor, a sub-set of which are shown below:

270
$$CH_3C(O)O_2 + CH_3O_2 \quad \rightarrow \quad CH_3CO_2 + CH_3O + O_2 \qquad \text{(R30)}$$

$$CH_3C(O)O_2 + CH_3C(O)O_2 \quad \rightarrow \quad 2\,CH_3CO_2 + O_2 \qquad \text{(R31)}$$

$$CH_3O_2 + CH_3O_2 \quad \rightarrow \quad 2\,CH_3O + O_2 \qquad \text{(R32)}$$

$$CH_3O + O_2 \quad \rightarrow \quad HO_2 + HCHO \qquad \text{(R33)}$$

$$HO_2 + HO_2 \quad \rightarrow \quad H_2O_2 + O_2 \qquad \text{(R34)}.$$

275   The CH_3CO_2 thermally decompose in air to form CH_3 and CO_2 (R21a) so that $CH_3C(O)O_2$, CH_3O_2 and HO_2 are initially present. HO_2, formed in R33 reacts with all organic peroxy radicals in both radical termination and radical propagation steps:

$$CH_3C(O)O_2 + HO_2 \qquad \rightarrow \qquad CH_3C(O)OOH + O_2 \qquad\qquad (R35)$$

$$\rightarrow \qquad CH_3C(O)OH + O_3 \qquad\qquad (R36)$$

$$\rightarrow \qquad OH + CH_3 + O_2 + CO_2 \qquad\qquad (R37)$$

280   $$CH_3O_2 + HO_2 \qquad \rightarrow \qquad CH_3OOH + O_2 \qquad\qquad (R38).$$

The OH formed in reaction R37 will react with acetone (which is present in large excess) to form another peroxy radcial:

$$OH + CH_3C(O)CH_3 + O_2 \qquad \rightarrow \qquad CH_3C(O)CH_2O_2 + H_2O \qquad\qquad (R39).$$

The acetonyl peroxy radical ($CH_3C(O)CH_2O_2$) will also undergo reaction with other RO_2, eventually forming peroxides and C1 and C2-peroxyl radicals. In summary, the chemistry taking place in the PAN-photochemical source generates a large variety

285   of oxidised organic trace gases (not only PAN) that may enter the TD-inlet at 648 K. Of particular interest with respect to explaining the data of Fig. 2 are the thermally unstable peroxides such as $CH_3C(O)OOH$, CH_3OOH and H_2O_2. These trace gases are stable at room temperature but have lifetimes with respect to thermal dissociation to OH of 0.06 s (Sahetchian et al., 1992), 0.6 s (Kirk, 1965) and 41 s (Yang et al., 2021) at 648 K, respectively.

The thermal dissociation of $CH_3C(O)OOH$ in the TD-inlet leads (via the thermal dissociation of initially formed CH_3CO_2

290   (R21)) to the formation of an OH radical and CH_3O_2 (R40) (Schmidt and Sehon, 1963; Atkinson et al., 2006):

$$CH_3C(O)OOH\ (+ O_2) \qquad \rightarrow \qquad CH_3O_2 + CO_2 + OH \qquad\qquad (R40).$$

The CH_3O_2 thus formed can, via reactions R22 and R23, account for some of the conversion of NO to NO_2 observed. However, both R23 and R40 generate OH radicals, which can react with acetone in the TD-inlet. The rate coefficient for OH + acetone at 648 K is 1.4×10^{-12} cm^3 molecule^{-1} s^{-1} (Vasudevan et al., 2005) which results in an OH-lifetime in the heated inlet of ~ 1 ms

295   with respect to reaction with acetone. This results in the formation of the acetonyl peroxy radical (R39) which then also reacts with NO (R41) to form other peroxyl radicals (HO_2, $CH_3C(O)O_2$ and CH_3O_2 via reactions R42 and R43) that can also convert NO to NO_2.

$$CH_3C(O)CH_2O_2 + NO \qquad \rightarrow \qquad CH_3C(O)CH_2O + NO_2 \qquad\qquad (R41)$$

$$CH_3C(O)CH_2O + O_2 \qquad \rightarrow \qquad CH_3C(O)CHO + HO_2 \qquad\qquad (R42)$$

300   $$CH_3C(O)CH_2O + \Delta H\ (+ O_2) \qquad \rightarrow \qquad CH_3C(O)O_2 + HCHO \qquad\qquad (R43)$$

The hypothesised role of the thermal dissociation of $CH_3C(O)OOH$ and H_2O_2 at 648 K as source of peroxyl radicals in the TD-inlet was tested by flowing $CH_3C(O)OOH$ (~ 1 ppbv) or H_2O_2 (2 – 10 ppmv, calculated from vapour pressure) sample through the TD-inlet in the presence of various amounts of NO (Fig. 4). Note that the NO_2 measured in the room temperature cavity

305   (present as an impurity of 3.5 % in the NO bottle) has been subtracted from the data obtained in the 648 K TD-inlet. As can be seen in Fig. 4a, the addition of up to 17.5 ppbv NO to 1 ppbv PAA or 2-10 ppmv H_2O_2 results in 0.6 ppbv or 5 ppbv NO_2, respectively, confirming that the thermal decomposition of PAA and H_2O_2 at 648 K is a source of peroxyl radicals. The

hypothesis was further tested by varying the TD-inlet temperature when flowing either PAA or H_2O_2 in the presence of 12 ppbv NO. As shown in Fig. 4b, in both cases we observed efficient conversion of NO to NO_2 at temperatures above 500 K for

310 PAA and above 400 K for H_2O_2. In separate experiments, we observed that the thermal dissociation of acetone also accounts for a small fraction of the overestimation NO_2 formed (400 pptv NO_2 at 43 ppmv acetone and 16 ppbv NO), which is confirmed by its thermogram (Fig. S2).

In order to gain insight into the identity and relative concentrations of the trace gases exiting the photochemical reactor, two sets of numerical simulations were carried out with FACSIMILE (Curtis and Sweetenham, 1987), both with and without the

315 addition of NO to the photochemical PAN source (i.e. with and without PAN formation, Tab. S1). The results are summarised in Fig. S3 which displays the evolution of products in the photochemical reactor as a function of time. At 89 ppbv NO (Fig S3a) 88 ppbv PAN is produced. Note that, following dilution, this would result in ~ 2 ppbv of acetone in the TD-inlets as observed experimentally. The simulation indicates ppmv mixing ratios of several organic traces gases in the photochemical reactor with 570 ppmv HCHO, 60 ppmv CH_3OOH and 1 ppmv H_2O_2 after 120 s reaction time. In the absence of NO (and thus

320 PAN, Fig. S3b) higher mixing ratios of these organics are generated, as expected. In this case the simulation predicts 1650 ppmv HCHO, 125 ppmv CH_3OOH, 37 ppmv $CH_3C(O)CH_2O_2$, 15 ppmv PAA and 2 ppmv H_2O_2.

In summary, the photochemical PAN source is not well suited for characterising the inlet chemistry for alkyl nitrate detection via thermal decomposition to NO_2 as it results in significant NO to NO_2 conversion owing to the presence of thermally labile trace gases such as peracetic acid and hydrogen peroxide. The presence of organic acids and their possible interference in

325 chemical-ionisation mass spectrometric studies of PAN has been documentde previously (Mielke and Osthoff, 2012).

4.2 The influence of NO and NO_2 on the measurement of PNs (PAN diffusion source)

The results presented above clearly demonstrate that the photochemical PAN source generates not only PAN but a number of oxidised organics that can influence the chemistry in the TD-inlet. This precludes an accurate assessment of the bias caused by the presence of NO or NO_2 when attempting to measure ΣPNs in real air masses. For this reason, further experiments were

330 performed with a PAN diffusion source which is not expected to have any significant impurities. The IR spectrum (Fig. S4) of a gas sample eluted from the PAN diffusion source is in good agreement with the literature and does not reveal the presence of high levels of impurities.

Figure 5 shows the results of three experiments in which PAN was added to zero air at mixing ratios of 2.0 and 6.5 ppbv and detected (following thermal dissociation) in both the 448 K and 648 K inlets as NO_2. As described in the experiments above,

335 the addition of various amounts of NO to the inlet results in a strong positive bias to the measurement, with a factor ~2 more NO_2 measured at 15 ppbv NO. Compared to the photochemical PAN source the bias (NO_2 formed per ppbv NO added) is smaller, which is related to the absence of impurities such as $CH_3C(O)OOH$. The solid lines in these plots are the results of numerical simulations that consider the formation and loss of radicals (both gas-phase and heterogeneous) in the TD-inlets and the resultant oxidation of NO to NO_2. The simulations are described in detail in previous publications from this group (Sobanski

340 et al., 2016; Thieser et al., 2016). While the simulations reproduce the bias caused by NO oxidation to NO_2 reasonably well in

these laboratory experiments with only one major trace-gas present (PAN) apart from NO, the situation in the real atmosphere will be more complex with potentially several different PAN species and many other trace gases that also interact with OH in the TD-inlets to form other peroxyl radicals that may react with NO.

An effective approach to remove the bias caused by NO oxidation to NO_2 has been described for a TD-inlet system in this

345   group, designed to detect NO_y via conversion to NO_2 (Friedrich et al., 2020). In this case, the air exiting the TD-inlet is allowed to cool before adding sufficient O_3 to convert NO to NO_2 (see section 3.1) and PAN is measured as NO_X rather than NO_2. The results of an experiment in which PAN was detected as NO_X is displayed as the red and blue lines in Fig. 5. In this case, ~3.7 ppbv PAN were initially present and up to 17 ppbv of NO were added. The clear dependence of the retrieved PAN mixing ratio on the NO mixing ratio is no longer apparent when using either the 448 K or 648 K TD-inlet and alleviates the need to

350   perform numerical simulations to correct the data.

The bias caused by the recombination of NO_2 with $CH_3C(O)O_2$ (section 2) was investigated when both NO_2 and NO_X were detected. The results of two experiments in which either 2.0 or 6.5 ppbv PAN from the diffusion source were sampled into the TD-CRDS with the addition of various amount of NO_2 are shown in Fig. 6. The effect of the recombination of the acetyl peroxy radical with NO_2 at 448 K can be seen in the data. Initial mixing ratios of PAN of 2.0 ppbv and 6.5 ppbv are only

355   detected as 1.1 ppbv and 3.4 ppbv NO_2, respectively. At 648 K the effect is significantly smaller than at 448 K, reflecting the thermal instability of $CH_3C(O)O_2$ at the higher temperature. The solid black and grey lines in this plot are the results of numerical simulations (Sobanski et al., 2016; Thieser et al., 2016). For the detection of NO_X (blue and red symbols in Fig. 6) a similar effect was observed as for the detection of NO_2. Thus, numerical simulations are still required to correct for the bias caused by the oxidation of NO_2. Within the experimental uncertainty, there is no significant difference in the size of the

360   negative bias when detecting PAN as either NO_2 or NO_X. This is readily understandable, as the recombination of $CH_3C(O)O_2$ with NO_2 to reform PAN after the gas flow cools down (after the heated inlets) is not influenced by the presence of O_3 which is added later.

4.3 Influence of NO on the measurement of ∑ANs

As described in section 2, a saturated, C3-alkyl-nitrate (IPN) has been widely used to characterise instruments using thermal

365   dissociation to convert alkyl nitrates to (detectable) NO_2. In previous work (Dewald et al., 2021), we have shown how IPN differs in its TD-inlet chemistry from biogenically derived, unsaturated nitrates which undergo surface catalysed reactions (e.g. with ozone) on hot quartz surfaces at 448 K, resulting in the unwanted detection of ANs in the PNs channel and a bias to measurements obtained in environments dominated by biogenic nitrates. Dewald et al. (2021), were able to remove this effect in their measurements of ΣPNs by using a 448 K inlet made of PFA rather than quartz. The instrument still however suffered

370   from the positive bias caused by reactions of peroxyl radicals with NO, which was enhanced compared to a quartz inlet, as the RO_2 radical losses to the PFA-tubing were reduced. Correction of the data obtained with that configuration thus required numerical simulations, which were based on laboratory experiments using IPN (Sobanski et al., 2016; Thieser et al., 2016;

Ohara et al., 2024). We have extended these experiments by using atmospherically more relevant (unsaturated) alkyl nitrates formed by the NO_3-initiated degradation of isoprene and limonene.

375 The results of experiments in which either 0.47 or 4.4 ppbv isoprene nitrate (derived by mixing N_2O_5 with isoprene in a reaction chamber, see section 3.3) was sampled into the TD-CRDS with the addition of various amounts of NO are illustrated in Fig. 7a. In these experiments, either NO_X (blue symbols) or NO_2 (i.e. the O_3 source was switched off, orange symbols) was measured. For the "NO_2-mode" experiments NO_2 was present at (14.8 ± 0.2) ppbv which is a consequence of using N_2O_5 in the chamber to generate NO_3.

380 In the "NO_2-mode" experiment using isoprene derived nitrate, the addition of ~ 22 ppbv of NO results in a doubling of the NO_2 signal (factor 2.3). This contrasts the results of Thieser et al. (2016), who, using IPN as surrogate alkyl-nitrate observed larger effects as represented by the black line in Fig. 7a (Thieser et al., 2016).

For limonene derived nitrate(s), the bias when measuring in "NO_2-mode" is very large with the addition of the same amount of NO (22 ppbv) resulting in a 690 % overestimation of LIMO-NIT (in the presence of (19.3 ± 0.2) ppbv NO_2). This contrasts

385 previous results from this group obtained using IPN as surrogate alkyl-nitrate and observed much smaller effects which are represented by the black line in Fig. 7b (Thieser et al., 2016). In summary, at a NO mixing ratio of 20 ppbv (and NO_2 ~ 20 ppbv), the fractional conversion of NO to NO_2 per 1 ppb of AN present in the sample flow is 7.0 % for IPN, 5.1 % for ISOP-NIT and 25 % for LIMO-NIT. Clearly, the conversion of NO to NO_2 in the heated TD-inlet is not only dependent on the amount of NO available to react but also on the nature of the alkyl nitrate. This result is partially intuitive, as the secondary

390 chemistry resulting from degradation of the longer chain alkyl nitrates will generate more organic peroxy radicals (to oxidize NO to NO_2) than IPN. In order to gain some insight into the secondary chemistry involved, numerical simulations of the laboratory data were conducted. The starting point was the reaction scheme used to correct the PNs data as described previously. Rather than attempt to simulate all of the processes occuring at 648 K in the TD-inlet (for which rate coefficients are not available) we varied the number of peroxy radicals generated from the decomposition of the alkoxy radicals formed

395 in the first reaction of the biogenic derived RO_2 with NO and allowed them to react with NO at a rate coefficient of $2.55 \times 10^{-12} \times \exp(380/T)$ cm^3 molecule^{-1} s^{-1}).

$$\text{LIMO/ISOP-NIT} + \Delta H \quad \rightarrow \quad NO_2 + RO \quad \text{(R44)}$$
$$RO + O_2 \quad \rightarrow \quad n\,RO_2 \quad \text{(R45)}$$
$$RO_2 + NO \quad \rightarrow \quad RO + NO_2 \quad \text{(R46)}$$
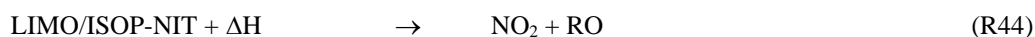
400 To approximately simulate the data, a value of $n = 1$ was sufficient for isoprene nitrate, whereas a value of 5 was required to reproduce the very large effect observed for limonene nitrate. This is related to the different number of carbon atoms and chemical structure and the different chemical reactions in the presence of NO in the TD-inlet. From our results, it is apparent, that 1) IPN is not a suitable surrogate molecule for the correction of $\sum$ANs, as has previously been practised and 2) given that ambient measurements will normally mixture of many alkyl nitrates, corrections based on numerical simulations that have

405 been optimised for IPN will not provide reliable data unless NO levels are very low.

Experiments in "NO_X-mode" (Fig. 7, blue symbols) in which 22.5 ppbv NO was added to either limonene nitrates (Fig. 7b) or isoprene nitrate (Fig. 7a, both formed by the reaction of NO_3 and the corresponding terpene) in the simulation chamber were also conducted and the results are strikingly different to those when NO_2 was detected. As expected, there is no significant dependence on NO added between zero and 22 ppbv.

5 Conclusions

We have shown that the use of a conventional, photochemical (acetone based) source of PAN can result in incorrect chacterisation of TD-inlets when used to detect PANs and ANs. This is caused by the presence of thermally labile, peroxidic trace gases, which lead to a strong positive bias of NO to NO_2 conversion in the ANs inlet. The use of "pure" PAN samples is considered to be superior as it results in more accurate themograms and NO dependencies in the heated inlet designed to detect ANs.

For the first time, we have investigated the potential bias from secondary chemistry (e.g. oxidation of ambient NO to NO_2) when using biogenic nitrates derived from terpenoids. The results indicate a larger bias for limonene nitrates and a smaller bias for isoprene nitrates than obtained using a saturated organic nitrate such as IPN. While IPN has the undoubted advantage of being commercialy available and easy to handle, its use to characterise TD-inlets to detect ANs will not lead to results that can be transferred to other (longer chain) nitrates as has been frequently performed. The effect is partially understood in terms of the sequential breakdown of the C10 backbone (e.g. for terpenes) to peroxy radicals that convert NO to NO_2.

Inspired by the success of our instrument to detect inorganic and organic NO_Y species as NO_x subsequent to thermal dissociation (Friedrich et al., 2020) we have modified our PANs / ANs instrument in a similar manner (i.e. by detecting NO_X rather than NO_2). The results indicate that, when sampling the real atmosphere with NO present, this mode of operation is to be preferred over NO_2 detection as the positive bias caused when RO_2 formed e.g. from biogenic precursors reacts with ambient NO is eliminated.

In the instrument configuration described here with the PANs TD-inlet made of PFA, the ANs TD-inlet made of quartz and the addition of O_3 downstream of the TD-inlets to convert NO to NO_2 corrections for the oxidation of NO by O_3 and RO_2 is no longer necessary and channel cross-talk (i.e. the detection of a fraction of ANs at the PANs inlet) is avoided. The only requirement for simulation is to remove the (negative) bias caused by the recombination of acyl peroxy radicals with NO_2 downstream of the TD-inlets. As the dominant atmospheric acyl peroxy nitrate is PAN itself, for which detailed experiments exist to characterise the system, this does not introduce significant uncertainty into the measurement of ΣPNs unless NO_2 levels are very large.

6 Author contribution

435 LW and PD performed the experiments, GT assisted with development and deployment of NO_3 sources and data acquisition. LW evaluated the data and wrote the first draft of the manuscript. JC conceptualised the SCHARK experiments and with JL contributed to the manuscript. This study was carried out in part fulfilment of the PhD of LW at the Johannes Gutenberg University Mainz.

7 Competing Interests

440 The authors declare that they have no conflict of interest.

8 Acknowledgements

445 ## 9 References

Atkinson, R., Baulch, D. L., Cox, R. A., Crowley, J. N., Hampson, R. F., Hynes, R. G., Jenkin, M. E., Rossi, M. J., and Troe, J.: Evaluated kinetic and photochemical data for atmospheric chemistry: Volume II - reactions of organic species, Atmos. Chem. Phys., 3625-4055, doi:10.5194/acp-6-3625-2006, 2006.

Brown, S. S., Stark, H., Ryerson, T. B., Williams, E. J., Nicks, D. K., Trainer, M., Fehsenfeld, F. C., and Ravishankara, A. R.:
450 Nitrogen oxides in the nocturnal boundary layer: Simultaneous in situ measurements of NO_3, N_2O_5, NO_2, NO, and O_3, J. Geophys. Res. -Atmos., 108, art. 4299, doi:10.1029/2002JD002917, 2003.

Brown, S. S., and Stutz, J.: Nighttime radical observations and chemistry, Chem. Soc. Rev., 41, 6405–6447, 2012.

Carr, S. A., Baeza-Romero, M. T., Blitz, M. A., Pilling, M. J., Heard, D. E., and Seakins, P. W.: OH yields from the CH_3CO+O_2 reaction using an internal standard, Chem. Phys. Lett., 445, 108-112, 2007.

455 Carr, S. A., Glowacki, D. R., Liang, C.-H., Baeza-Romero, M. T., Blitz, M. A., Pilling, M. J., and Seakins, P. W.: Experimental and modeling studies of the pressure and temperature dependences of the kinetics and the OH yields in the acetyl + O_2 reaction, J. Phys. Chem. A, 115, 1069-1085, 2011.

Chen, S.-Y., and Lee, Y.-P.: Transient infrared absorption of t-$CH_3C(O)OO$, c-$CH_3C(O)OO$, and α-lactone recorded in gaseous reactions of CH_3CO and O_2, J. Chem. Phys., 132, 114303, doi:doi: 10.1063/1.3352315, 2010.

460 Crutzen, P. J.: The role of NO and NO_2 in the chemistry of the troposphere and stratosphere, Ann. Rev. Earth Planet. Sci., 7, 443-472, 1979.

Curtis, A. R., and Sweetenham, W. P.: Facsimile, Atomic Energy Research Establishment, Report R-12805, Facsimile, Atomic Energy Research Establishment, Report R-12805, 1987.

Day, D. A., Wooldridge, P. J., Dillon, M. B., Thornton, J. A., and Cohen, R. C.: A thermal dissociation laser-induced
465 fluorescence instrument for in situ detection of NO_2, peroxy nitrates, alkyl nitrates, and HNO_3, J. Geophys. Res. -Atmos., 107, doi:doi:10.1029/2001jd000779, 2002.

Dewald, P., Dörich, R., Schuladen, J., Lelieveld, J., and Crowley, J. N.: Impact of ozone and inlet design on the quantification of isoprene-derived organic nitrates by thermal dissociation cavity ring-down spectroscopy (TD-CRDS), Atmos. Meas. Tech., 14, 5501-5519, doi:10.5194/amt-14-5501-2021, 2021.

470 Dewald, P., Nussbaumer, C. M., Schuladen, J., Ringsdorf, A., Edtbauer, A., Fischer, H., Williams, J., Lelieveld, J., and Crowley, J. N.: Fate of the nitrate radical at the summit of a semi-rural mountain site in Germany assessed with direct reactivity measurements, Atmos. Chem. Phys., 22, 7051-7069, doi:10.5194/acp-22-7051-2022, 2022.

Dewald, P., Seubert, T., Andersen, S. T., Türk, G. N. T. E., Schuladen, J., McGillen, M. R., Denjean, C., Etienne, J. C., Garrouste, O., Jamar, M., Harb, S., Cirtog, M., Michoud, V., Cazaunau, M., Bergé, A., Cantrell, C., Dusanter, S., Picquet-475 Varrault, B., Kukui, A., Xue, C., Mellouki, A., Lelieveld, J., and Crowley, J. N.: NO$_3$ reactivity during a summer period in a temperate forest below and above the canopy, Atmos. Chem. Phys., 24, 8983-8997, doi:10.5194/acp-24-8983-2024, 2024.

Di Carlo, P., Aruffo, E., Busilacchio, M., Giammaria, F., Dari-Salisburgo, C., Biancofiore, F., Visconti, G., Lee, J., Moller, S., Reeves, C. E., Bauguitte, S., Forster, G., Jones, R. L., and Ouyang, B.: Aircraft based four-channel thermal dissociation laser induced fluorescence instrument for simultaneous measurements of NO$_2$, total peroxy nitrate, total alkyl nitrate, and 480 HNO$_3$, Atmos. Meas. Tech., 6, 971-980, doi:10.5194/amt-6-971-2013, 2013.

Flocke, F. M., Weinheimer, A. J., Swanson, A. L., Roberts, J. M., Schmitt, R., and Shertz, S.: On the measurement of PANs by gas chromatography and electron capture detection, J. Atmos. Chem., 52, 19-43, 2005.

Friedrich, N., Tadic, I., Schuladen, J., Brooks, J., Darbyshire, E., Drewnick, F., Fischer, H., Lelieveld, J., and Crowley, J. N.: Measurement of NOx and NOy with a thermal dissociation cavity ring-down spectrometer (TD-CRDS): instrument 485 characterisation and first deployment, Atmos. Meas. Tech., 13, 5739-5761, doi:10.5194/amt-13-5739-2020, 2020.

Gaffney, J. S., Fajer, R., and Senum, G. I.: An improved procedure for high-purity gaseous peroxyacyl nitrate production - use of heavy lipid solvents, Atmos. Env., 18, 215-218, doi:Doi 10.1016/0004-6981(84)90245-2, 1984.

Geyer, A., Ackermann, R., Dubois, R., Lohrmann, B., Muller, T., and Platt, U.: Long-term observation of nitrate radicals in the continental boundary layer near Berlin, Atmos. Env., 35, 3619-3631, doi:10.1016/S1352-2310(00)00549-5, 2001.

490 Groß, C. B. M., Dillon, T. J., Schuster, G., Lelieveld, J., and Crowley, J. N.: Direct Kinetic Study of OH and O3 Formation in the Reaction of CH3C(O)O2 with HO2, The Journal of Physical Chemistry A, 118, 974-985, doi:10.1021/jp412380z, 2014.

Heintz, F., Platt, U., Flentje, H., and Dubois, R.: Long-term observation of nitrate radicals at the tor station, Kap Arkona (Rugen), J. Geophys. Res. -Atmos., 101, 22891-22910, 1996.

Horowitz, L. W., Fiore, A. M., Milly, G. P., Cohen, R. C., Perring, A., Wooldridge, P. J., Hess, P. G., Emmons, L. K., and 495 Lamarque, J.-F.: Observational constraints on the chemistry of isoprene nitrates over the eastern United States, J. Geophys. Res., 112, D12S08-, 2007.

Keehan, N. I., Brownwood, B., Marsavin, A., Day, D. A., and Fry, J. L.: A thermal-dissociation–cavity ring-down spectrometer (TD-CRDS) for the detection of organic nitrates in gas and particle phases, Atmos. Meas. Tech., 13, 6255-6269, doi:10.5194/amt-13-6255-2020, 2020.

500 Kirk, A. D.: The thermal decomposition of methyl hydroperoxide, Can. J. Chem., 43, 2236-2242, 1965.

Lambe, A. T., Bai, B., Takeuchi, M., Orwat, N., Zimmerman, P. M., Alton, M. W., Ng, N. L., Freedman, A., Claflin, M. S., Gentner, D. R., Worsnop, D. R., and Liu, P.: Technical note: Gas-phase nitrate radical generation via irradiation of aerated ceric ammonium nitrate mixtures, Atmos. Chem. Phys., 23, 13869-13882, doi:10.5194/acp-23-13869-2023, 2023.

Lee, J., Chen, C.-J., and Bozzelli, J. W.: Thermochemical and kinetic analysis of the acetyl radical (CH$_3$CO) + O$_2$ Reaction 505 System, J. Phys. Chem. A, 106, 7155-7170, doi:doi:10.1021/jp014443g, 2002.

Lee, L., Wooldridge, P. J., Gilman, J. B., Warneke, C., de Gouw, J., and Cohen, R. C.: Low temperatures enhance organic nitrate formation: evidence from observations in the 2012 Uintah Basin Winter Ozone Study, Atmos. Chem. Phys., 14, 12441-12454, doi:doi:10.5194/acp-14-12441-2014, 2014.

Lelieveld, J., Evans, J. S., Fnais, M., Giannadaki, D., and Pozzer, A.: The contribution of outdoor air pollution sources to
510 premature mortality on a global scale, Nature, 525, 367-371, doi:10.1038/nature15371, 2015.

Li, C., Wang, H., Chen, X., Zhai, T., Chen, S., Li, X., Zeng, L., and Lu, K.: Thermal dissociation cavity-enhanced absorption
spectrometer for measuring NO_2, RO_2NO_2, and $RONO_2$ in the atmosphere, Atmos. Meas. Tech., 14, 4033-4051,
doi:10.5194/amt-14-4033-2021, 2021.

Liebmann, J., Karu, E., Sobanski, N., Schuladen, J., Ehn, M., Schallhart, S., Quéléver, L., Hellen, H., Hakola, H., Hoffmann,
515 T., Williams, J., Fischer, H., Lelieveld, J., and Crowley, J. N.: Direct measurement of NO_3 radical reactivity in a boreal forest,
Atmospheric Chemistry and Physics 2018, 3799-3815, doi:10.5194/acp-18-3799-2018, 2018.

Liebmann, J., Sobanski, N., Schuladen, J., Karu, E., Hellén, H., Hakola, H., Zha, Q., Ehn, M., Riva, M., Heikkinen, L.,
Williams, J., Fischer, H., Lelieveld, J., and Crowley, J. N.: Alkyl nitrates in the boreal forest: formation via the NO3-, OH-
and O3-induced oxidation of biogenic volatile organic compounds and ambient lifetimes, Atmos. Chem. Phys., 19, 10391-
520 10403, doi:10.5194/acp-19-10391-2019, 2019.

Lightfoot, P. D., Cox, R. A., Crowley, J. N., Destriau, M., Hayman, G. D., Jenkin, M. E., Moortgat, G. K., and Zabel, F.:
Organic Peroxy-radicals - Kinetics, Spectroscopy and Tropospheric Chemistry, Atmos. Env. A, 26, 1805-1961, 1992.

Lin, C., Hu, R., Xie, P., Zhang, G., Liu, X., Tong, J., and Liu, W.: A three-channel thermal dissociation cavity ring-down
spectrometer for simultaneous measurement of ambient total peroxy nitrates, total alkyl nitrates, and NO_2, Talanta, 270,
525 125524, doi:https://doi.org/10.1016/j.talanta.2023.125524, 2024.

Mielke, L. H., and Osthoff, H. D.: On quantitative measurements of peroxycarboxylic nitric anhydride mixing ratios by thermal
dissociation chemical ionization mass spectrometry, Int. J. Mass Spectrom., 310, 1-9,
doi:https://doi.org/10.1016/j.ijms.2011.10.005, 2012.

Murphy, J. G., Thornton, J. A., Wooldridge, P. J., Day, D. A., Rosen, R. S., Cantrell, C., Shetter, R. E., Lefer, B., and Cohen,
530 R. C.: Measurements of the sum of HO_2NO_2 and $CH_3O_2NO_2$ in the remote troposphere, Atmos. Chem. Phys., 4, 377-384,
2004.

Ng, N. L., Brown, S. S., Archibald, A. T., Atlas, E., Cohen, R. C., Crowley, J. N., Day, D. A., Donahue, N. M., Fry, J. L.,
Fuchs, H., Griffin, R. J., Guzman, M. I., Herrmann, H., Hodzic, A., Iinuma, Y., Jimenez, J. L., Kiendler-Scharr, A., Lee, B.
H., Luecken, D. J., Mao, J., McLaren, R., Mutzel, A., Osthoff, H. D., Ouyang, B., Picquet-Varrault, B., Platt, U., Pye, H. O.
535 T., Rudich, Y., Schwantes, R. H., Shiraiwa, M., Stutz, J., Thornton, J. A., Tilgner, A., Williams, B. J., and Zaveri, R. A.:
Nitrate radicals and biogenic volatile organic compounds: oxidation, mechanisms, and organic aerosol, Atmos. Chem. Phys.,
17, 2103-2162, doi:10.5194/acp-17-2103-2017, 2017.

Ohara, N., Shioji, T., Matsumoto, J., Inomata, S., Sakamoto, Y., Kajii, Y., Shiigi, H., and Sadanaga, Y.: Improved continuous
measurement system for atmospheric total peroxy and total organic nitrate under the high NOx condition, Rev. Sci. Instrum.,
540 95, doi:10.1063/5.0172219, 2024.

Orlando, J. J., and Tyndall, G. S.: Laboratory studies of organic peroxy radical chemistry: an overview with emphasis on recent
issues of atmospheric significance, Chem. Soc. Rev., 41, 6294-6317, 2012.

Papadimitriou, V. C., Karafas, E. S., Gierczak, T., and Burkholder, J. B.: $CH_3CO + O_2 + M$ (M = He, N_2) reaction rate
coefficient measurements and implications for the OH radical product yield, J. Phys. Chem. A, 119, 7481-7497,
545 doi:doi:10.1021/acs.jpca.5b00762, 2015.

Paul, D., Furgeson, A., and Osthoff, H. D.: Measurements of total peroxy and alkyl nitrate abundances in laboratory-generated
gas samples by thermal dissociation cavity ring-down spectroscopy, Rev. Sci. Instrum., 80, Art. 114101,
doi:10.1063/1.3258204 2009.

Paul, D., and Osthoff, H. D.: Absolute Measurements of Total Peroxy Nitrate Mixing Ratios by Thermal Dissociation Blue
550 Diode Laser Cavity Ring-Down Spectroscopy, Anal. Chem., 82, 6695-6703, doi:doi:10.1021/ac101441z, 2010.

Perring, A. E., Pusede, S. E., and Cohen, R. C.: An observational perspective on the atmospheric impacts of alkyl and multifunctional nitrates on ozone and secondary organic aerosol, Chem. Rev., 113, 5848-5870, doi:doi:10.1021/cr300520x, 2013.

Roberts, J. M.: The atmospheric chemistry of organic nitrates, Atmos. Environ., Part A, 24, 243-287, doi:10.1016/0960-555 1686(90)90108-y, 1990.

Sadanaga, Y., Takaji, R., Ishiyama, A., Nakajima, K., Matsuki, A., and Bandow, H.: Thermal dissociation cavity attenuated phase shift spectroscopy for continuous measurement of total peroxy and organic nitrates in the clean atmosphere, Rev. Sci. Instrum., 87, doi:10.1063/1.4958167, 2016.

Sahetchian, K. A., Rigny, R., Tardieu de Maleissye, J., Batt, L., Anwar Khan, M., and Mathews, S.: The pyrolysis of organic 560 hydroperoxides (ROOH), Symposium (International) on Combustion, 24, 637-643, doi:https://doi.org/10.1016/S0082-0784(06)80078-0, 1992.

Schmidt, C., and Sehon, A. H.: Themal decomposition of peracetic acid in vapor phase, Canadian Journal of Chemistry-Revue Canadienne De Chimie, 41, 1819-&, doi:10.1139/v63-261, 1963.

Slusher, D. L., Huey, L. G., Tanner, D. J., Chen, G., Davis, D. D., Buhr, M., Nowak, J. B., Eisele, F. L., Kosciuch, E., Mauldin, 565 R. L., Lefer, B. L., Shetter, R. E., and Dibb, J. E.: Measurements of pernitric acid at the South Pole during ISCAT 2000, Geophys. Res. Lett., 29, Art. 2011, doi:doi:10.1029/2002gl015703, 2002.

Slusher, D. L., Huey, L. G., Tanner, D. J., Flocke, F. M., and Roberts, J. M.: A thermal dissociation-chemical ionization mass spectrometry (TD-CIMS) technique for the simultaneous measurement of peroxyacyl nitrates and dinitrogen pentoxide, J. Geophys. Res. -Atmos., 109, Art Nr. D19315, doi:10.1029/2004JD004670, 2004.

570 Sobanski, N., Schuladen, J., Schuster, G., Lelieveld, J., and Crowley, J. N.: A five-channel cavity ring-down spectrometer for the detection of NO_2, NO_3, N_2O_5, total peroxy nitrates and total alkyl nitrates, Atmos. Meas. Tech., 9, 5103-5118, doi:10.5194/amt-9-5103-2016, 2016.

Spittler, M., Barnes, I., Bejan, I., Brockmann, K. J., Benter, T., and Wirtz, K.: Reactions of NO_3 radicals with limonene and alpha-pinene: Product and SOA formation, Atmos. Env., 40, S116-S127, doi:10.1016/j.atmosenv.2005.09.093, 2006.

575 Taha, Y. M., Saowapon, M. T., Assad, F. V., Ye, C. Z., Chen, X., Garner, N. M., and Osthoff, H. D.: Quantification of peroxynitric acid and peroxyacyl nitrates using an ethane-based thermal dissociation peroxy radical chemical amplification cavity ring-down spectrometer, Atmos. Meas. Tech., 11, 4109-4127, doi:10.5194/amt-11-4109-2018, 2018.

Talukdar, R. K., Burkholder, J. B., Schmoltner, A. M., Roberts, J. M., Wilson, R. R., and Ravishankara, A. R.: Investigation of the loss processes for peroxyacetyl nitrate in the atmosphere: UV photolysis and reaction with OH, J. Geophys. Res. -580 Atmos., 100, 14163-14173, doi:doi:10.1029/95jd00545, 1995.

Thieser, J., Schuster, G., Phillips, G. J., Reiffs, A., Parchatka, U., Pöhler, D., Lelieveld, J., and Crowley, J. N.: A two-channel, thermal dissociation cavity-ringdown spectrometer for the detection of ambient NO_2, RO_2NO_2 and $RONO_2$, Atmos. Meas. Tech., 9, 553-576, doi:10.5194/amt-9-553-2016, 2016.

Tyndall, G. S., Staffelbach, T. A., Orlando, J. J., and Calvert, J. G.: Rate coefficients for the reactions of OH radicals with 585 methylglyoxal and acetaldehyde, Int. J. Chem. Kinet., 27, 1009-1020, 1995.

Vandaele, A. C., Hermans, C., Simon, P. C., Carleer, M., Colin, R., Fally, S., Merienne, M. F., Jenouvrier, A., and Coquart, B.: Measurements of the NO_2 absorption cross-section from 42 000 cm^{-1} to 10 000 cm^{-1} (238-1000 nm) at 220 K and 294 K, J. Quant. Spectrosc. Radiat. Transfer, 59, 171-184, 1998.

Vasudevan, V., Davidson, D. F., and Hanson, R. K.: High temperature measurements of the reactions of OH with toluene and 590 acetone, J. Phys. Chem., 109, 3352-3359, 2005.

Warneck, P., and Zerbach, T.: Synthesis of peroxyacetyl nitrate in air by acetone photolysis, Env. Sci. Tech., 26, 74-79, 1992.

Wayne, R. P., Barnes, I., Biggs, P., Burrows, J. P., Canosa-Mas, C. E., Hjorth, J., Le Bras, G., Moortgat, G. K., Perner, D., Poulet, G., Restelli, G., and Sidebottom, H.: The nitrate radical: Physics, chemistry, and the atmosphere, Atmos. Env. A, 25A, 1-206, 1991.

595 Wooldridge, P. J., Perring, A. E., Bertram, T. H., Flocke, F. M., Roberts, J. M., Singh, H. B., Huey, L. G., Thornton, J. A., Wolfe, G. M., Murphy, J. G., Fry, J. L., Rollins, A. W., LaFranchi, B. W., and Cohen, R. C.: Total Peroxy Nitrates (ΣPNs) in the atmosphere: the Thermal Dissociation-Laser Induced Fluorescence (TD-LIF) technique and comparisons to speciated PAN measurements, Atmos. Meas. Tech., 3, 593-607, doi:doi:10.5194/amt-3-593-2010, 2010.

Wu, R., Vereecken, L., Tsiligiannis, E., Kang, S., Albrecht, S. R., Hantschke, L., Zhao, D., Novelli, A., Fuchs, H., Tillmann, 600 R., Hohaus, T., Carlsson, P. T. M., Shenolikar, J., Bernard, F., Crowley, J. N., Fry, J. L., Brownwood, B., Thornton, J. A., Brown, S. S., Kiendler-Scharr, A., Wahner, A., Hallquist, M., and Mentel, T. F.: Molecular composition and volatility of multi-generation products formed from isoprene oxidation by nitrate radical, Atmos. Chem. Phys., 21, 10799-10824, doi:10.5194/acp-21-10799-2021, 2021.

Yang, X., Shen, X., Zhao, P., and Law, C. K.: Statistical Analysis on Rate Parameters of the H2–O2 Reaction System, The 605 Journal of Physical Chemistry A, 125, 10223-10234, doi:10.1021/acs.jpca.1c08250, 2021.

Zheng, W., Flocke, F. M., Tyndall, G. S., Swanson, A., Orlando, J. J., Roberts, J. M., Huey, L. G., and Tanner, D. J.: Characterization of a thermal decomposition chemical ionization mass spectrometer for the measurement of peroxy acyl nitrates (PANs) in the atmosphere, Atmos. Chem. Phys., 11, 6529-6547, 2011.

610 **10 Figures**
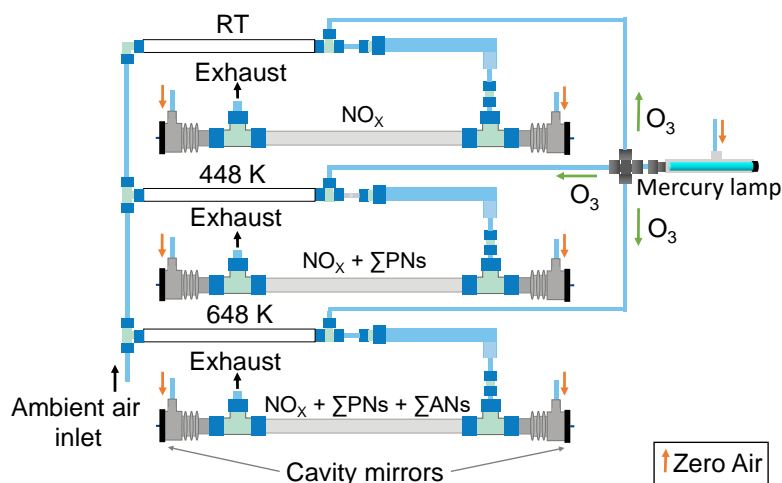
Figure 1: Schematic representation of the 409 nm cavities of the 5-channel TD-CRDS for measuring mixing ratios of NO$_X$, NO$_X$ + ΣPNs and NO$_X$ + ΣPNS + ΣANs (Hg-lamp on). Alternatively, when the Hg-lamp is off NO$_2$ is measured instead of NO$_X$. The coloured arrows 615 represent the gas flows. The temperatures of the different TD-inlets (measured at the outside surface) are shown for each channel.
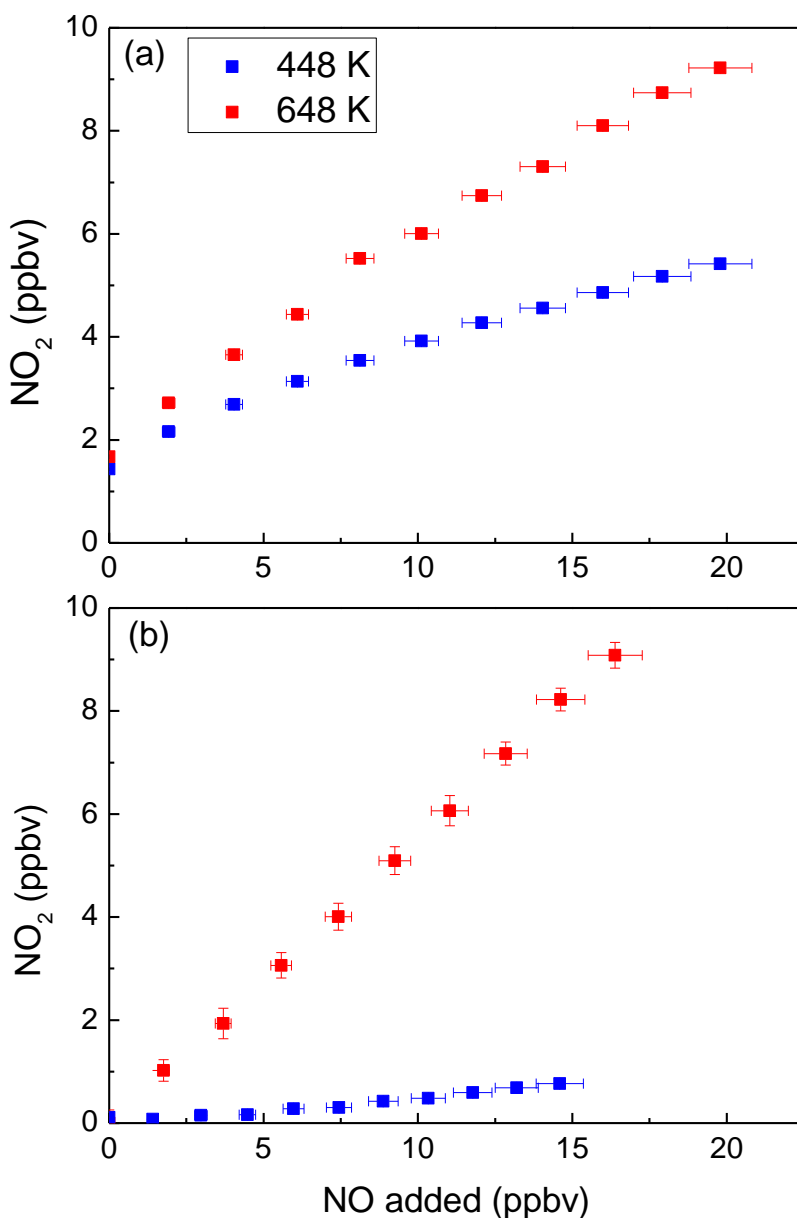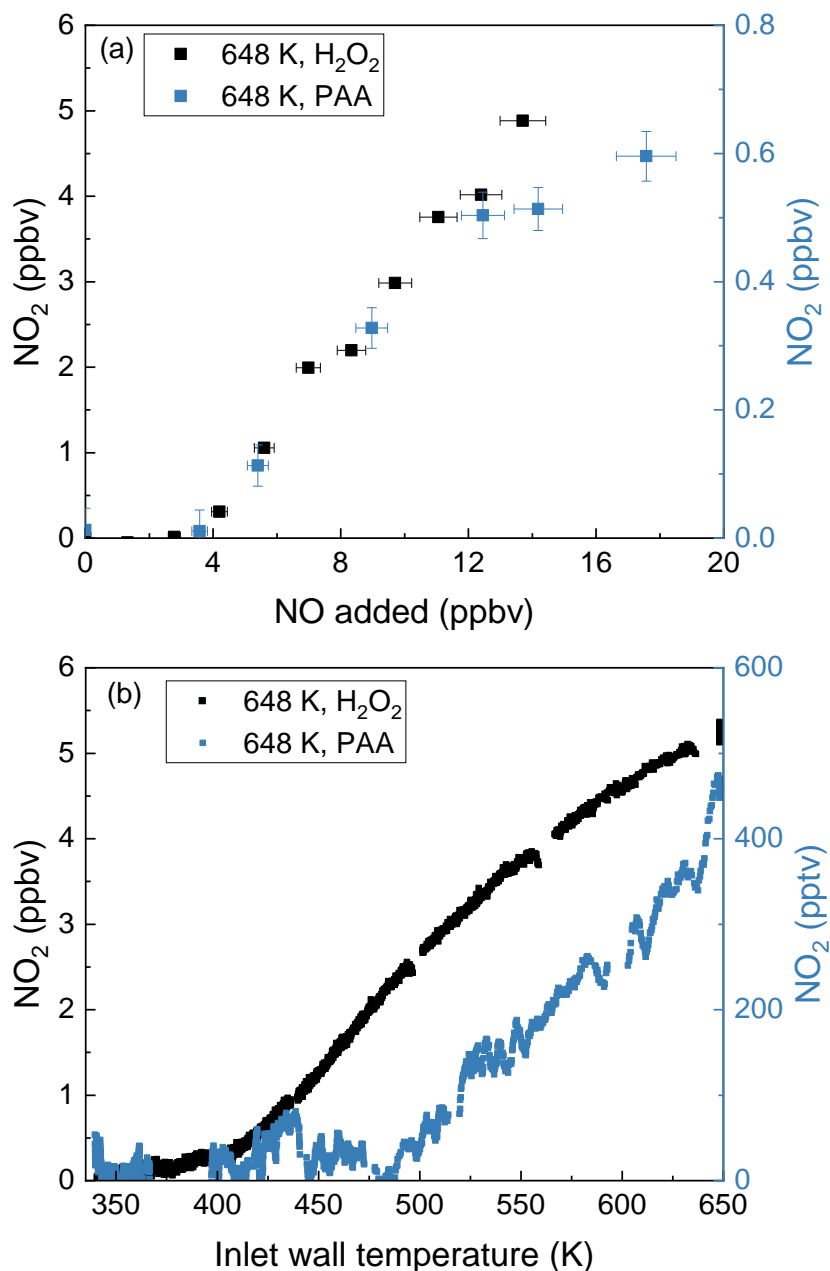
Figure 2: **(a)** NO$_2$ measured in the cavities with inlet temperatures of 448 K and 648 K while adding NO to photochemically produced PAN. The error bars in the x-direction include uncertainty in the mass flow controllers (1 % of the maximum flow of the MFC) and the uncertainty in the mixing ratio of the NO bottle (5 %). The error bars in the y-direction include the standard deviations (1 σ) of the NO$_2$ mixing ratios both at 648 K and at room temperature. **(b)** Same as panel (a) but without NO flow into the photochemical PAN source (i.e. no PAN formation).
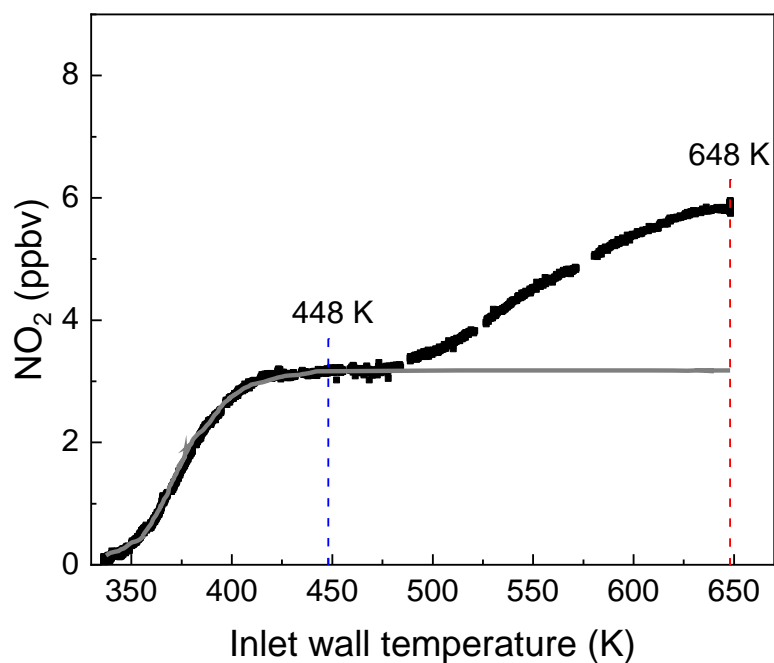
Figure 3: Thermogram obtained by adding 13 ppbv NO to 1 ppbv PAN from the photochemical PAN source. The vertical red and blue lines
625 indicate the normal operating temperatures of the two heated inlets associated with the $\sum$ANs and $\sum$PNs cavities, respectively. Note that the
NO_2 measured in the room temperature cavity (impurity present in the NO and PAN flows) has already been subtracted. The grey line
represents the expected thermogram for PAN (i.e. no increase after full dissociation at ~450 K).

Figure 4: (a) NO$_2$ measured in the cavity with an inlet temperature at 648 K while adding NO to PAA ($\approx$ 1 ppbv) and H$_2$O$_2$ (2 – 10 ppmv). The error bars in the x-direction accounts for uncertainty in the mass flows (1 % of the maximum flow of the MFC) and the uncertainty of the mixing ratio of the NO bottle (5 %). The error bars in the y-direction account for uncertainty (1 σ) in the NO$_2$ mixing ratios both at 648 K and at room temperature. **(b)** Thermograms measured in the ANs-cavity while adding 12 ppbv NO to PAA ($\approx$ 0.3 ppbv) and H$_2$O$_2$ (2 – 10 ppmv).

23
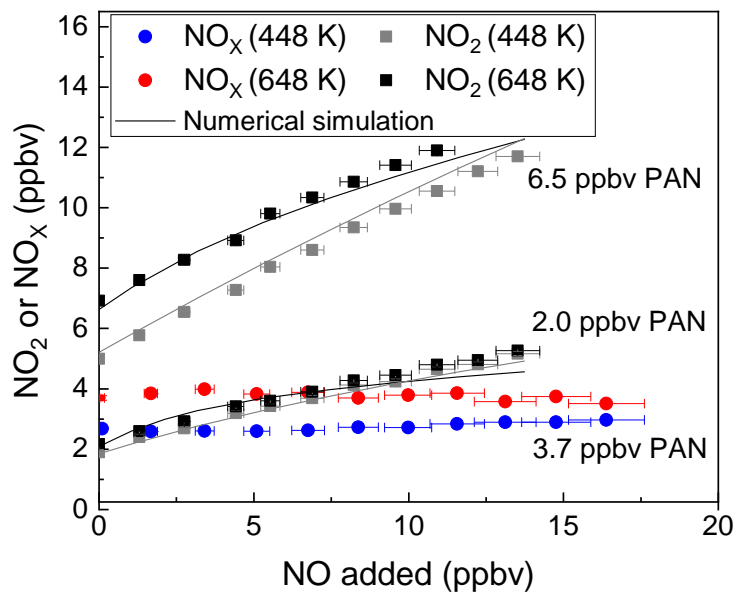
Figure 5: Measured mixing ratios of NO_2 and NO_X during the addition of NO to PAN from the diffusion source for the cavities with inlet temperatures of 448 K and 648 K. The error bars in the x-direction consider uncertainty in the mass flows (1 % of the maximum flow of the MFC) and uncertainty in the mixing ratio of the NO bottle (5 %). The error bars in the y-direction for 448 K consider the standard deviations (1 σ) of the NO_2 mixing ratios both at 448 K and at room temperature. The error bars in the y-direction for 648 K account for the standard deviations (1 σ) of the NO_2 mixing ratios both at 648 K and at room temperature The black and grey solid lines show the numerical simulation.
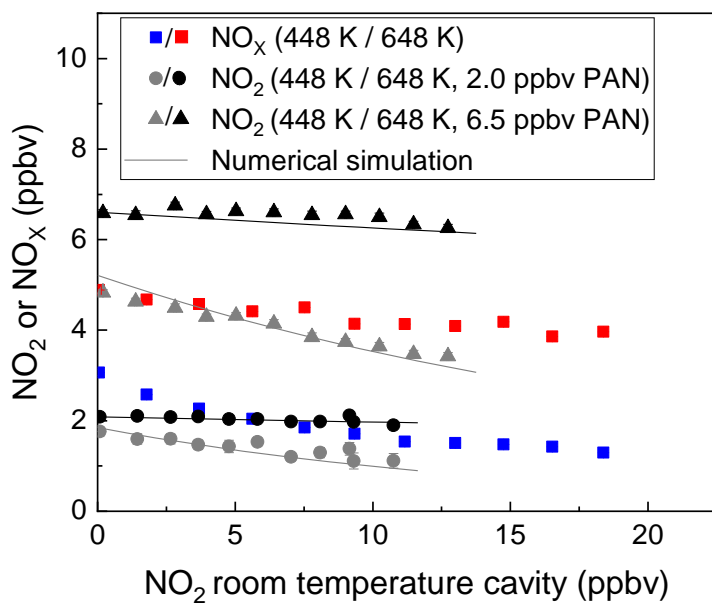
Figure 6: Measured mixing ratios of NO_X and NO_2 during the addition of NO_2 (measured with the cavity with inlet at room temperature) to PAN from the diffusion source. The inlet temperatures were 448 K and 648 K. The error bars in the x-direction represent standard deviation (1 σ) of the NO_2 mixing ratio at room temperature, those in the y-direction for 648 K account for uncertainty (1 σ) in the NO_2 mixing ratios both at 648 K and at room temperature. The error bars in the y-direction for 448 K account for the standard deviations (1 σ) of the NO_2 mixing ratios both at 448 K and at room temperature. The black and grey solid lines are the results of numerical simulations.
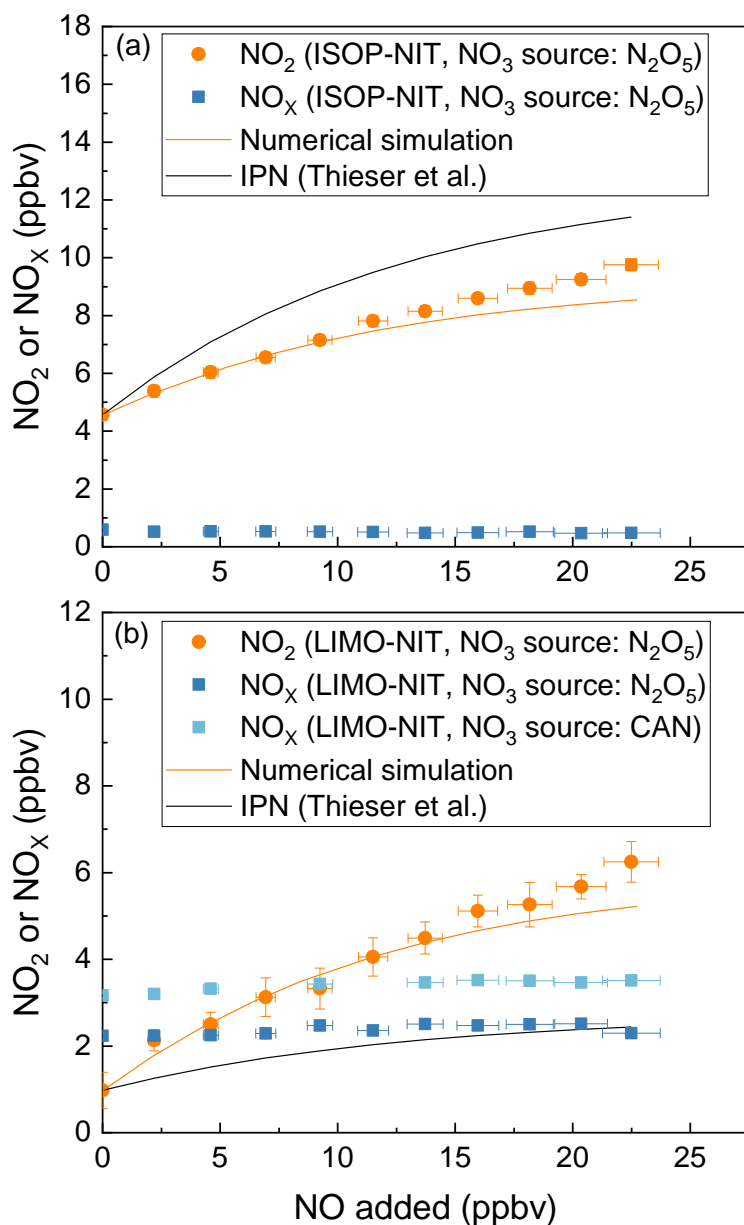
Figure 7: Addition of NO to flowing samples of either **(a)** isoprene derived nitrates (ISOP-NIT) or **(b)** limonene derived nitrates (LIMO-NIT). NO$_3$ was either generated with an N$_2$O$_5$ diffusion source or via cerium(IV) ammonium nitrate photolysis (CAN). The error bars in the x-direction consider uncertainty in the mass flows (1 % of the maximum flow of the MFC) and uncertainty in the mixing ratio of the NO bottle (5 %). The error bars in the y-direction consider the standard deviations (1 σ) of the NO$_2$ mixing ratios both at 648 K and at room temperature. The orange lines are the results of numerical simulations of the data at 648 K. The black lines are calculated from the expression: NO$_2$ = 1 + 1.8(exp(-0.08 · NO(ppbv)) (Thieser et al., 2016) as derived for addition of NO to IPN. The NO$_2$ or NO$_X$ measured in the room temperature cavity has been subtracted from that measured in the cavity associated with the 648 K TD-inlet.